NANO LETTERS

2007
Vol. 7, No. 12
3822−3826

Patterned When Wet: Environment-Dependent Multifunctional Patterns within Amphiphilic Colloidal Crystals

Adrian M. Brozell, Michelle A. Muha, Arian Abed-Amoli, Daniel Bricarello, and Atul N. Parikh*

Departments of Applied Science and Biophysics Graduate Group, University of California, Davis, California 95616

Received September 27, 2007; Revised Manuscript Received October 20, 2007

ABSTRACT

A simple integration of molecular and colloidal self-assembly approaches with photopatterning is shown to produce multifunctional patterns of amphiphilic colloidal crystals. These crystals display binary spatial patterns of wettability by water and a single photonic stop-band in air. Upon exposure to water, the uniform stop-band is replaced by a pattern of coexisting stop-bands that reflect the underlying pattern of surface wetting. These hydration-dependent photonic patterns within single colloidal crystals form because of near-complete water rejection from the three-dimensionally disposed nanoscale interstices in hydrophobic regions and its exclusive permeation within the hydrophilic regions. This water permeation pattern is further structured by the three-dimensional (3D) distribution and contiguity of the nanoscale interstices between individual colloids, allowing 3D patterned organization of functional units in secondary self-assembly processes, as illustrated using quantum dots, metal nanoparticles, and fluorescent probes.

Morpho butterfly wings integrate structural color and superhydrophobic "Lotus-effect" to simultaneously produce environment dependent, brilliant iridescence, and highly efficient water-repellency.[1−3] Synthetic materials that integrate such widely disparate optical and wetting properties within single monolithic structures are difficult to produce.[4−6] In the work reported here, we show that by combining molecular and colloidal self-assembly with photopatterning, multifunctional patterns of amphiphilic colloidal crystals can be routinely produced. These crystals display binary spatial patterns of superwettability by water[7,8] and a single photonic stop-gap[9−11] in air. Upon immersion in water, this uniform stop-band is replaced by a pattern of coexisting stop-bands that reflect the underlying pattern of surface wetting. This hydration-dependent photonic patterns within single colloidal crystals form because of near-complete water rejection from the three dimensional (3D) interstices in hydrophobic regions. Furthermore, the selective water permeation pattern compartmentalizes subsequent solution-phase chemistries, also structured by the 3D distribution and contiguity of the interstices between individual colloids, as illustrated by the 3D-patterned organization of quantum dots, nanoparticles, and fluorescent molecules.

Planar colloidal crystals (pCCs) obtained by spontaneous self-assembly provides a natural starting point for achieving structural color.[11] Using nanoscale beads, they afford three-dimensionally periodic, spatial variations in dielectric properties on the order of the wavelengths of light. Bragg diffraction of light within photonic crystals gives rise to a stop-band, or a pseudogap, in which the propagation of light within a narrow range of wavelengths and in specific directions is prohibited.[12] We used the well-known physical confinement method[13] to self-assemble submicrometer-sized monodisperse, hydrophilic silica (SiO_2) beads into 3D pCCs on planar glass slides. Here, an aqueous-phase, concentrated colloidal sol is sandwiched between a hydrophilic and a hydrophobic glass plate, and solvent is allowed to evaporate. The capillary condensation drives the formation of a 3D pCCs over large, macroscopic areas (∼cms). Following this procedure, multilamellar pCC thin-films of controlled thicknesses (a few to several thousand layers) in a substantially uniform, close-packed cubic organization with (111) plane parallel to the substrate surface can be routinely produced (Figure 1a).

The individual beads comprising the crystal are subsequently rendered hydrophobic by solution (or vapor) phase self-assembly of alkyl ($CH_3(CH_2)_{17}SiCl_3$, *n*-octadecyl trichlorosilane, OTS) or fluoroalkyl ($F_3C(CF_2)_7C_2H_4SiCl_3$, 1H,1H,-2H,2H perfluoro decyltricholorosilane, FDTS) molecules

* Corresponding author. Phone: (530) 754-7055. Fax: (530) 752-2444. E-mail: anparikh@ucdavis.edu.

10.1021/nl072483b CCC: $37.00
Published on Web 11/10/2007

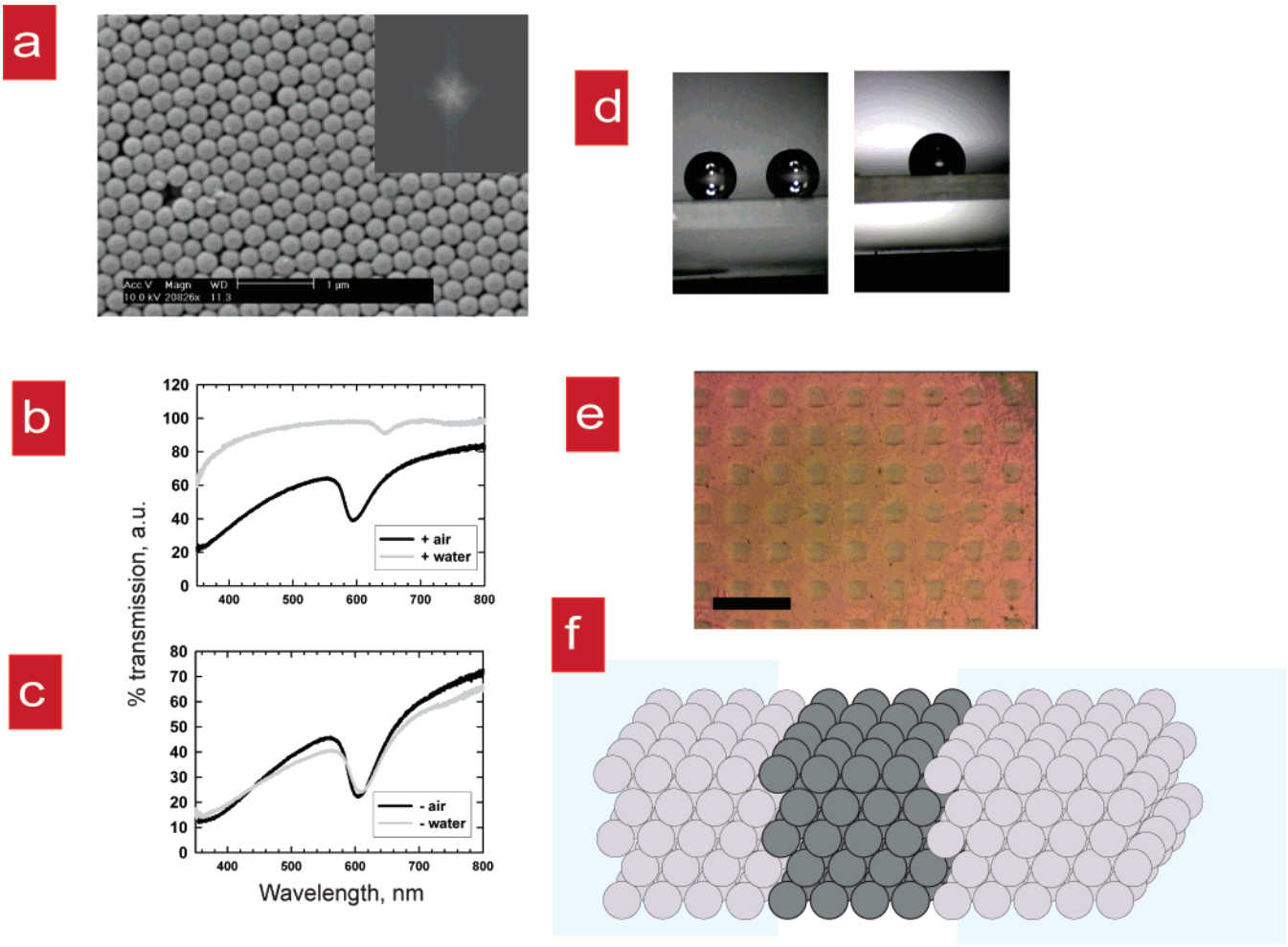

Figure 1. Amphiphilic planar colloidal crystals. (a) A typical SEM image of pCC (274 nm silica colloids). (Inset) Fourier transform of the image. (b−c) Representative UV−vis spectra of hydrophilic pCC in air (λ_m, 592.8 nm; fwhm, ($\Delta\lambda$) 40.6 nm) and in water (λ_m, 645.0 nm; $\Delta\lambda$, 25.6 nm) and (c) hydrophobised (silanised) pCC in air (λ_m, 602.8 nm; $\Delta\lambda$, 36.0 nm) and in water (λ_m, 611.2 nm; $\Delta\lambda$,36.8 nm). (d) Optical images of 5 μL water drop on FDTS derivatized (−) pCC (left) and planar glass slide (right). (e) A color optical image of a wet amphiphilic colloidal crystal: +, square; −, grid. The scale bar is 200 μm. (f) A cartoon summary of amphiphilic planar colloidal crystal (pCC) showing water permeation (blue) in and expulsion from the interstices surrounding hydrophilic (+) and hydrophobic (−) regions respectively.

(silanisation).[14] These self-assembled monolayers neutralize surface charge on silica beads (~4.8e nm^{-2}) and produce a ~2.0−2.5 nm coatings terminated with hydrophobic methyl (−CH_3) or fluoromethyl (−CF_3) functional groups on the beads. The silanisation process does not perturb the 3D structural order, and the corresponding photonic stop-band of the pCCs as confirmed by their nominally unchanged spectral properties and SEM images. Surface wetting characteristics of silanised pCCs are however significantly altered. As seen in Figure 1b, optical images of water drops reveal high contact angles, measured at 127 (±2) and 138° (±2°), for OTS and FDTS derivatized pCCs, which is notably higher than 103 (±2) and 110° (±2°) obtained for OTS and FDTS derivatized flat glass surfaces. This enhanced water repellancy reflects a coupling of nanoscale periodic topography of the crystal surface with the local hydrophobic character of individual silanised beads.[15]

In air, both hydrophilic and silanised pCCs are brightly colored due to their structurally defined optical stop-band. For hydrophilic crystals derived using 274 (±6) nm silica beads, the stop-band is manifest in the appearance of a characteristic dip at 594 ± 2 nm (full width at half maximum, fwhm, ~40 nm) in normal optical transmission measurements (Figure 1c). This transmission dip is well described by Bragg's condition for the wavelengths of normal incidence light-diffracted away from the propagation direction. The position of this minima agree well with the Bragg's peak ($\lambda_{max} = 2n_{eff}d$ where d is the interlayer repeat distance ($\sqrt{}$-(2/3) × colloid diameter) *and* n_{eff} represents the effective refractive index of the medium) estimate of 603 nm for face-centered cubic (fcc) packing (filling fraction, 0.74) of 274 nm silica ($n_{SiO_2} = 1.45$) colloids. The ~40 nm width of the transmission peak is consistent with previous observations of limiting or intrinsic widths for pCCs and attributed to the strong diffraction from near surface planes.[16]

When submerged in water, the spectra of hydrophilic pCCs show (1) a reversible shift in position from 594 ± 2 nm to 643 ± 2 nm; (2) a narrowing of the diffraction peak from 40 ± 2 nm to 27 ± 2 nm; and (3) an increase in the transmission percentage (Figure 1c). These shifts in ampli-

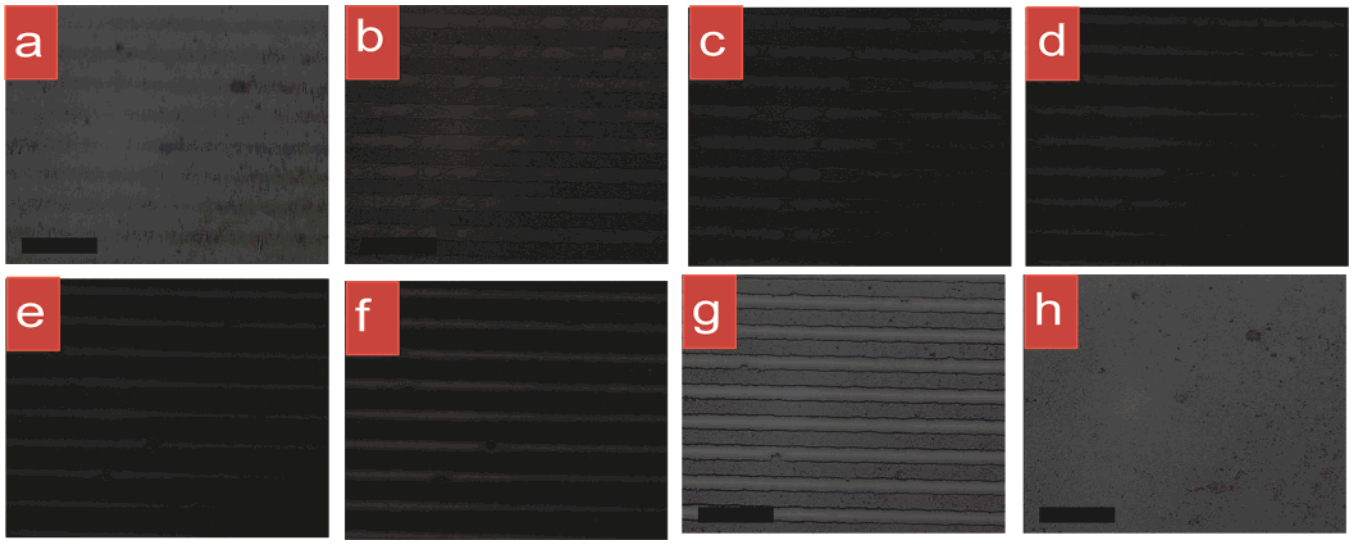

Figure 2. Breath figures. Selected frames from a time-lapse movie of water condensation in (a−f) and evaporation from (g−h) in an amphiphilic pCC (274 nm silica colloids). Frames are 10 s apart. Scale bar = 100 μm

tude, width, and positions of the transmission dip correspond well with the change in refractive index contrast following the replacement of interstitial air by water in hydrophilic colloidal crystals. These hydration-induced changes are entirely reversible: redrying the wetted samples reproduces the original stop-band properties. Because the structural properties of pCCs do not change upon immersion in water (as assessed by the reversible changes in optical properties following repeated drying and rehydration), the precise locations of the stop-band in air and water can be used within Bragg's law to simultaneously solve for n_{eff} and d. This simple analysis yields an estimate of 63% for the effective packing density (compared to 74% for a defect-free fcc configuration) and interplanar distance of 0.83D (compared to 0.816D for an fcc packing) where D is the nominal particle diameter. This 11% lower packing density is not unreasonable because of defects and drying-induced shrinkages common in pCCs formed by physical confinement.[17] In a marked contrast, hydrophobic pCCs submerged in water show no measurable shift in the position or the width of the stop-band (Figure 1d). This invariance in optical property is consistent with near-complete exclusion of water from the crystal interior composed of hydrophobic interfaces. Note that these hydrophobic pCCs consisting of silanised colloids are dominated by a close juxtaposition of a large number of hydrophobic surfaces, which in turn encapsulate nanoscale pores of tunable sizes. On the basis of these structural characteristics, hydrophobic pCCs should offer useful model systems to address long-standing issues surrounding the behaviors of water in confinement and at smooth and rough hydrophobic surfaces[18−22] and their practical consequences, for example, the nature and length scales of attractive forces between hydrophobic surfaces buried in water.

A particularly attractive feature of silane-derivatized hydrophobic pCCs is that the silane coating can be removed from beads in desired patterns using photolithography (Figure 1e,f). The aliphatic tails of OTS and FDTS from the surfaces of three-dimensionally dispersed beads within pCCs can be photolytically degraded in a spatially patterned manner determined by the two-dimensional (2D) mask pattern. We used short-wavelength UV radiation (187−254 nm) in conjunction with physical photomasks to transfer the 2D optical mask pattern into 3D chemical pattern within pCCs. This simple treatment concurrently produces within single pCCs corresponding relief patterns of (1) surface wettability; (2) water permeation pathways within the crystal interior; and (3) binary patterns of optical stop-bands.

The 3D amphiphilic pCCs display an orientation-dependent but optically uniform color when dry. Upon immersion in water, a striking optical pattern, reflecting the underlying pattern of surface wettability, emerges (Figure 1e). These patterns are reversibly erased upon subsequent drying of samples. This wetting-induced, reversible optical pattern formation can be straightforwardly ascribed to the change in the dielectric contrast resulting from water permeation in the hydrophilic region alone. These patterns of surface-wetting characteristics and water permeation pathways in single amphiphilic pCCs are most conveniently visualized using brightfield microscopy of time-dependent breath figures generated by exposure to water vapor. Selected frames from a time-lapse movie are shown in Figure 2. These images clearly reveal developing (and erasing) optical patterns due to selective condensation (or evaporation) of water in (or from) the hydrophilic regions of the pCC. These hydration-dependent patterns can be erased simply by reexposing the patterned pCCs to OTS (or FDTS) solution and new patterns written in subsequent UV photolithography steps. In this manner, hydration-dependent band gap patterns within single pCCs can be scribed and erased within single samples, which may be technologically useful in the development of photonic papers.[23]

The patterned infiltration of water in amphiphilic pCCs can be further exploited to compartmentalize fluid flow and aqueous phase chemistries[24] within the 3D contiguity of interstices in the hydrophilic regions of pCCs. Following this strategy, we demonstrate proof-of-principle experiments for

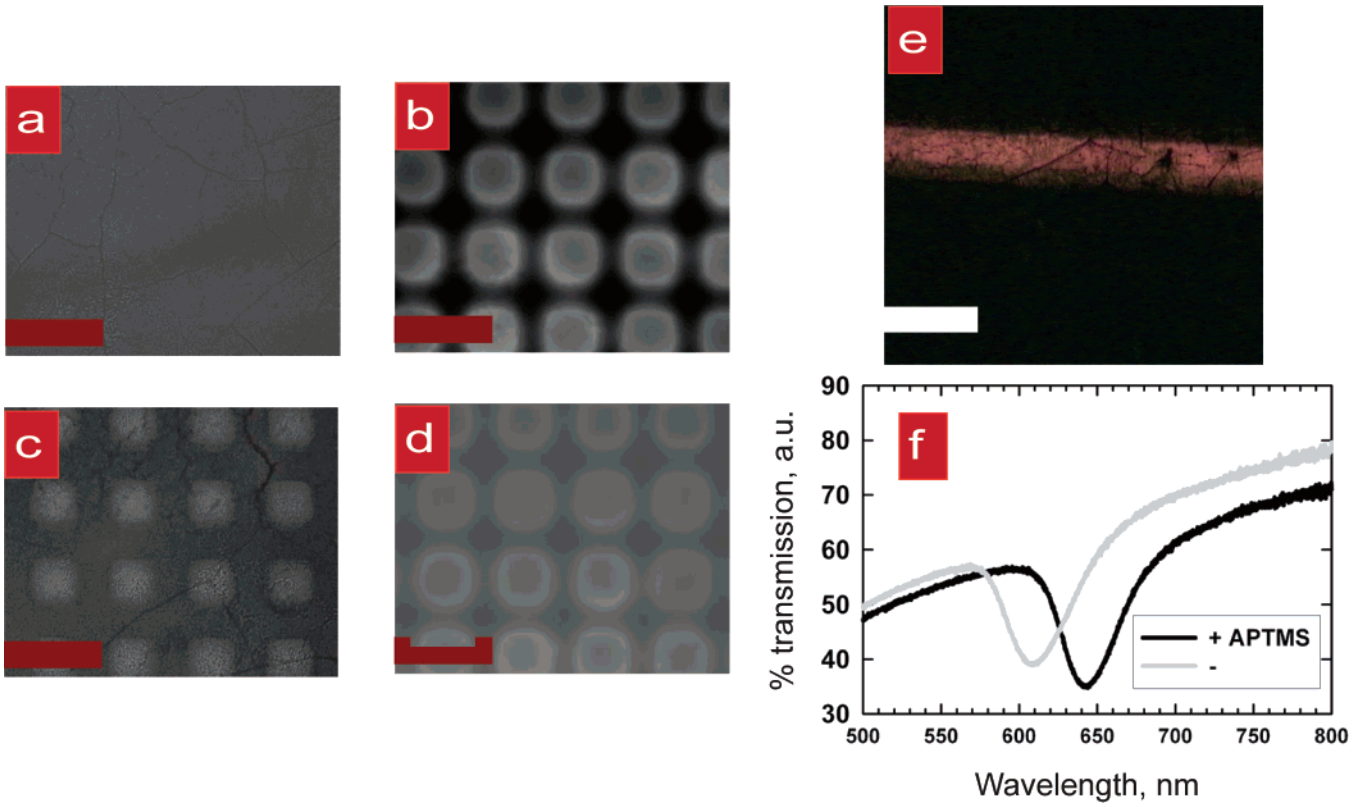

Figure 3. Patterned functionalities in a single colloidal crystal. (a−d) A brightfield (a) and epifluorescence (b) images of an amphiphilic (±) pCC in air following 24 h incubation with CdSe nanoparticles (QD). Corresponding brightfield (c) and epifluorescence (d) images in water. (Scale bar, 100 μm). (e) A color optical image of gold nanoparticles embedded in the hydrophilic regions of the colloidal crystal (Scale bar, 200 μm). (f) UV−vis spectra of hydrophilic (+) and hydrophobic (−) regions of an amphiphilic pCC after 24 h of reaction with APTMS (+: λ_m, 642.2 nm; $\Delta\lambda$, 39.0 nm. −: λ_m, 607.0 nm; $\Delta\lambda$, 37.2 nm).

applications in 3D-patterned organization of nanoparticles, self-assembling silane molecules, and optical fluorescent probes (and associated functionalities) as illustrated below. *First*, the amphiphilic pCCs can be used to embed quantum dots (QDs) and other nanoparticles in selective regions of the host pCCs. For QDs, the host lattices offer a control of interparticle spacing, surrounding microenvironment, and their meso- to microscale ordering that is important for their collective optical properties.[25] Furthermore, QD photoemission in the spectral region of the stop-band can be modulated, according to Fermi's golden rule for the local density of electromagnetic states,[12,25] opening up new possibilities for low-threshold microlasers and all-optical signal processing.[26] To begin to explore these applications, we expose amphiphilic pCCs comprising 274 nm silica beads to an aqueous solution (2 nM, 4 mL) of carboxy-terminated (COO^-), water-soluble, core−shell cadmium selenide (CdSe/ZnS, emission wavelength, 605 nm) QDs. Simply increasing the ionic-strength of the aqueous phase allows their salting out selectively into the hydrophilic regions of the pCCs (Figure 3). A comparison of wide-area bright-field images of an amphiphilic pCC confirms selective water permeation in hydrophilic pattern. Fluorescence and corresponding bright-field images shown in Figure 3 show bright emission at ~598 nm confirming the patterned depositions of QD particles within the hydrophilic interstices of the amphiphilic pCCs (Supporting Information, Figures 1 and 2). Confocal fluorescence microscopy data (Supporting Information, Figure 3) reveal that QD particles occupy the interstices three-dimensionally. Ongoing experiments will establish the optimal concentration of QD particles adsorbed within the host pCC patterns to maximize the modulation of QD spontaneous emission by the host stop-band and opening up of defect or transmission windows within the pCCs via patterned deposition of QD particles. Following this general strategy, metal nanoparticles (e.g., Au colloids, Figure 3e) and organic dyes can be deposited within the water permeation patterns of amphiphilic pCCs to engineer desired functional patterns.

Second, OTS and FDTS coatings on silanised beads present chemically inert surfaces toward many chemical reactions. As a result, such chemistries (even from organic solvents) can be confined to the hydrophilic regions of the colloidal crystal. This is illustrated by incubating a short-chain silane (3-aminopropyl trimethoxysilane, APTMS) in an organic solvent (toluene). The solution permeates through both the hydrophilic and hydrophobic regions of the crystal, but silanes react selectively with the silanols present on hydrophilic beads alone producing amino-terminated interstices within the parent hydrophilic patterns. Moreover, these amino termini can be subsequently derivatized to covalently link useful functionalities. An example is developed to demonstrate covalent coupling of pH dependent fluorescein in this fashion (Supporting Information, Figure 2). Further, by deliberately using APTMS incubation conditions known to produce thick coatings,[27] effective sizes of hydrophilic

colloids and correspondingly n_{eff} can be selectively increased thus permanently altering the associated stop-band properties. In Figure 3f, illustrative UV−vis spectra for the hydrophilic and hydrophobic regions of the APTMS-treated amphiphilic pCCs in air show the shift in the transmission dip to 642.2 nm in the hydrophilic region whereas hydrophobic regions of the amphiphilic pCCs remain unperturbed at 607.0 nm. Applying Bragg's law in conjunction with n_{eff} (=1.30) and d (=0.83D) deduced earlier, we estimate the effective bead diameter of 297 nm. This ~23 nm increase in bead thickness due to APTMS adsorption agrees well with that reported for APTMS adsorbed on planar glass under comparable incubation conditions.[27] This simple experiment indicates that the optical stop-band associated with hydrophilic region can be tuned and possibly fully erased (e.g., via silanisation or sol−gel-like processing in hydrophilic regions alone) thus opening up interesting opportunities to chemically engineer optical defects within single pCCs.[28]

Facile synthesis of amphiphilic planar colloidal crystals introduced here offers imminent opportunities to address critical issues in several disparate fields. First, is their use in highly parallel investigations of forces between hydrophobic surfaces, the structure of water at buried hydrophobic surfaces, and effects of confinement on fluids.[18] Second, the ability to systematically tune periodic tunable topography of the crystal surface and local chemistry should prove valuable in understanding superwetting behavior at surfaces.[7] Third, the formation of hydration-dependent stop-band patterns upon immersion in water suggests potential routes for photonic paper.[23] Fourth, extending spatially confined chemistry within colloidal interstices should allow the coupling of many technologically relevant optical and electronic functionalities to the photonic properties of host colloidal crystal lattices. Specifically, the approaches presented here should soon allow coupling of host-lattice optical properties with emission from embedded light sources in spatially defined patterns useful for optical devices and low threshold lasers.[25,26]

Acknowledgment. We thank B. Sanii for help with atomic force and confocal microscopy measurements. This paper integrates work performed under a grant from The Office of Science, U.S. Department of Energy (DE-FG02-04ER46173) and through U.S. NIH Roadmap for Medical Research via a Nanomedicince Center grant (National Center for Biomimetic Nanoconductors).

Supporting Information Available: Experimental methods. Figures and movies providing supporting data using confocal fluorescence, epifluorescence, and spectroscopy measurements. This information is available free of charge via Internet at http://pubs.acs.org.

References

(1) Barthlott, W.; Neinhuis, C. *Planta* **1997**, *202* (1), 1−8.
(2) Vukusic, P.; Sambles, J. R. *Nature* **2003**, *424* (6950), 852−855.
(3) Potyrailo, R. A.; Ghiradella, H.; Vertiatchikh, A.; Dovidenko, K.; Cournoyer, J. R.; Olson, E. *Nature Photonics* **2007**, *1* (2), 123−128.
(4) Parker, A. R.; Townley, H. E. *Nat. Nanotechnol.* **2007**, *2* (6), 347−353.
(5) Huang, J. Y.; Wang, X. D.; Wang, Z. L. *Nano Lett.* **2006**, *6* (10), 2325−2331.
(6) Gu, Z. Z.; Uetsuka, H.; Takahashi, K.; Nakajima, R.; Onishi, H.; Fujishima, A.; Sato, O. *Angew. Chem., Int. Ed.* **2003**, *42* (8), 894.
(7) Lafuma, A.; Quere, D. *Nat. Mater.* **2003**, *2* (7), 457−460.
(8) Oner, D.; McCarthy, T. J. *Langmuir* **2000**, *16* (20), 7777−7782.
(9) Colvin, V. L. *MRS Bulletin* **2001**, *26* (8), 637−641.
(10) Ozin, G. A.; Yang, S. M. *Adv. Funct. Mater.* **2001**, *11* (2), 95−104.
(11) Vlasov, Y. A.; Bo, X. Z.; Sturm, J. C.; Norris, D. J. *Nature* **2001**, *414* (6861), 289−293.
(12) Yablonovitch, E. *Phys. Rev. Lett.* **1987**, *58* (20), 2059−2062.
(13) Lu, Y.; Yin, Y. D.; Gates, B.; Xia, Y. N. *Langmuir* **2001**, *17* (20), 6344−6350.
(14) Sagiv, J. *J. Am. Chem. Soc.* **1980**, *102* (1), 92−98.
(15) Bico, J.; Marzolin, C.; Quere, D. *Europhys. Lett.* **1999**, *47* (2), 220−226.
(16) Bertone, J. F.; Jiang, P.; Hwang, K. S.; Mittleman, D. M.; Colvin, V. L. *Phys. Rev. Lett.* **1999**, *83* (2), 300−303.
(17) Gates, B.; Lu, Y.; Li, Z. Y.; Xia, Y. *Appl. Phys. A* **2003**, *76* (4), 509−513.
(18) Chandler, D. *Nature* **2005**, *437* (7059), 640−647.
(19) Doshi, D. A.; Watkins, E. B.; Israelachvili, J. N.; Majewski, J. *Proc. Natl. Acad. Sci. U.S.A.* **2005**, *102* (27), 9458−9462.
(20) Lum, K.; Chandler, D.; Weeks, J. D. *J. Phys. Chem. B* **1999**, *103* (22), 4570−4577.
(21) Poynor, A.; Hong, L.; Robinson, I. K.; Granick, S.; Zhang, Z.; Fenter, P. A. *Phys. Rev. Lett.* **2006**, *97*, (26).
(22) Singh, S.; Houston, J.; van Swol, F.; Brinker, C. J. *Nature* **2006**, *442* (7102), 526−526.
(23) Fudouzi, H.; Xia, Y. N. *Adv. Mater.* **2003**, *15* (11), 892−.
(24) Leopoldes, J.; Damman, P. *Nat. Mater.* **2006**, *5* (12), 957−961.
(25) Lodahl, P.; van Driel, A. F.; Nikolaev, I. S.; Irman, A.; Overgaag, K.; Vanmaekelbergh, D. L.; Vos, W. L. *Nature* **2004**, *430* (7000), 654−657.
(26) Noda, S. *Science* **2006**, *314* (5797), 260−261.
(27) Howarter, J. A.; Youngblood, J. P. *Langmuir* **2006**, *22* (26), 11142−11147.
(28) Braun, P. V.; Rinne, S. A.; Garcia-Santamaria, F. *Adv. Mater.* **2006**, *18* (20), 2665−2678.
(29) Frens, G. *Nat. Phys. Sci.* **1973**, *241* (105), 20−22.

NL072483B